Volume 1 | Number 1 | Jan 2013 | Pages 1–100

# Nanoscale

www.rsc.org/nanoscale

ROYAL SOCIETY OF CHEMISTRY

ROYAL SOCIETY OF CHEMISTRY

www.rsc.org/nanoscale

# TITLE

## Self-Powered Ion Detectors Based on Dye-Sensitized Photovoltaics

**AUTHORS:** *Kanika L. Agrawal[a] and Max Shtein[a, *]*

## ABSTRACT

Autonomous sensing of metal ion contamination in remote environments with high reproducibility and sensitivity could unlock many new applications, but involves trade-offs between compactness, sensitivity, and power provisioning. In prior demonstrations of semi-autonomous sensors, the power source (e.g. a solar cell) was an additional component. Here, we demonstrate a concept, wherein a dye-sensitized solar cell is used for both power generation and sensitive detection of ionic analytes, unlocking a new pathway for ultra-miniaturization and integration.

Selective and sensitive detection of metal ions is important in a wide variety of applications,[1-3] with but a few examples capable of measuring down to single nanomolar concentrations of charged species. Successful recent demonstrations include plasmonic resonance based energy transfer spectroscopy,[4] total internal reflection fluorescence spectroscopy,[5] photonic hydrogel based colorimetric detection[6] and other absorption/emission based techniques.[7] One major limitation for deploying such optical schemes in many intended applications is the need for complex auxiliary instrumentation, which is cumbersome, requires external power sources, and lacks robustness. Several chemotransistors have been developed to address this limitation; in these devices, an electrical signal is modulated in response to an analyte interacting with a variety of electrode and semiconductor materials, including graphene[8, 9] and organic polymers.[10, 11] Although requiring fewer components than optical detection schemes, chemotransistor-based detection of metal ions still requires an external power source. Some sensors incorporating photovoltaic cells as power sources have been demonstrated;[12] however, they are separate modules, increasing device cost and complexity. The need persists for compact, robust, and energy efficient ion detection with high sensitivity.

To address this need, we propose a sensing scheme in which the presence of ionic analytes disrupts (or triggers) the flow of electrical current between two electrodes, with the electromotive force ultimately provided by absorbed ambient light. Here we demonstrate an implementation of this concept, using the classical dye-sensitized solar cell structure consisting of cis-bis(isothiocyanato)bis(2,2′-bipyridyl-4,4′-dicarboxylato)-ruthenium (II) sensitizing dye (N3) and the iodide/triiodide redox shuttle.[13] We demonstrate the detection of $Ag^+$ ions, with high sensitivity and reproducibility, low cost and a compact form factor.

Since its inception,[14, 15] dye-sensitized solar cell (DSSC) technology has demonstrated adequate stability, low cost and ease of fabrication while being able to maintain competitive power conversion efficiencies for some applications. This platform is particularly compatible with detecting species in solution, because rapid charge transport in high efficiency DSSCs occurs in a liquid or gel electrolyte. For the proof-of-concept demonstration, we examine a 'turn off' type mode of operation where the presence of an ionic (or ionized) analyte shuts off photocurrent production. In this scheme, the device operates optimally to begin with and then sees a photocurrent drop in response to a detection event, such as adsorption of the analyte on to an electrode or quenching of the dye excited state. (**Fig. 1(a)** and **(b)**) The ionic target species can also be generated using an auxiliary release mechanism[16, 17] so as to allow for indirect detection of biological analytes.

Dye-sensitized solar cell devices were fabricated as per standard procedures, described in the supplemental information accompanying this article. The assembled devices were connected to a Solartron Analytical Modulab MTS Materials Test System and their electrical characteristics and impedance spectra were measured under 1 sun illumination and in the dark. A schematic representation of the testing procedure is shown in **Fig. 1(c)**. We performed identical tests on both, control devices, wherein a fixed volume of pure solvent was added to the device in addition to the electrolyte (**Fig. 1(d)**) and on the sensors, wherein silver nitrate dissolved in acetonitrile was injected into the device in addition to the electrolyte, at concentrations ranging from 1 nM to 10 mM. (**Fig. 1(e)**) The current density-voltage (J-V) characteristics for a typical device used in this study are shown in **Fig. 2(a)**; the inset shows the corresponding solar cell characterization parameters and material system employed; the caption lists essential performance characteristics.

The changes in device response in the presence of $Ag^+$ are shown in **Fig. 2(b)**. The practical utility of this scheme is manifested in the observation that the power conversion efficiency of the device never drops below 70% of its original value, thus ensuring that sufficient power is generated to modulate the intensity of an external circuit element even when a very high concentration of the analyte is present in the electrolyte. The $J_{SC}$ and $V_{OC}$ obtained from these measurements were plotted as a function of $Ag^+$ concentration (**Fig. 3**). A distinct drop in $J_{SC}$, accompanied by a steady increase in $V_{OC}$ was observed for concentrations of $Ag^+$ ranging between 1 μM and 1 mM. Concentrations of $Ag^+$ below 1 μM did not cause an appreciable change in the device characteristics, while concentrations greater than 1 mM caused the device to become resistive. We also performed electrochemical impedance spectroscopy (EIS) measurements and fitted the obtained data to an equivalent circuit model to obtain the resistances corresponding to electron recombination at the $TiO_2$/dye/electrolyte interface ($R_R$), and to charge transfer through the counter electrode ($R_{CT}$).[18, 19] (*see Supplementary Fig. 1*) As **Fig. 3(c)** and **(d)** show, there is a dramatic increase in both of these parameters with the addition of $Ag^+$, attributable to the formation of electrodeposited silver clusters and/or the reduction of silver iodide precipitate on the $TiO_2$ electrode to metallic silver under illumination. In both cases, charge transport is inhibited and the precipitate may render some dye sites inactive, while also blocking electron recombination at the $TiO_2$/dye/electrolyte interface.[20] A decrease in the reverse dark saturation current ($J_s$), extracted by fitting the observed data to the generalized Shockley model, qualitatively agrees with the hypothesis that the overall recombination rate is lowered with the addition of $Ag^+$. (*see Supplementary Fig. 2, 3*) This also supports the observed increase in $V_{OC}$, which can be described using the following equation:[21, 22]

$$V_{oc} = \frac{kT}{q} \ln \frac{J_{inj}}{(k_{rec} n_{c,0} [I_3^-])} \tag{1}$$

where k is the Boltzmann constant, T is the absolute temperature, q is the magnitude of the electron charge, $J_{inj}$ represents the injected electron flux, $k_{rec}$ is the recombination rate constant and $n_{c,0}$ is the density of conduction band electrons in the dark.

Energy-dispersive X-ray spectroscopy (EDS) was performed on the $TiO_2$ electrode following the $Ag^+$ sensing experiments, confirming the formation of silver clusters, as seen in **Fig. 4**. Furthermore, optical microscopy and scanning electron microscopy of the $TiO_2$ electrode revealed that a large proportion of the silver clusters are concentrated directly underneath the electrolyte-filling hole, due to the larger concentration driving force and a thinner boundary layer directly below the injection site. *(see Supplementary Fig. 4)* The limit of detection may be significantly improved by concentrating light in this region of the device, or by replacing the glass support for the counter electrode with a porous membrane that would eliminate the need for a filling hole, thereby allowing the analyte to interact homogenously with the entire device area.

To ensure that the dilution of the electrolyte by solvent addition and repeated electrolyte filling do not corrupt the test, we performed control tests. As the **insets** of **Figure 3** show, we found no substantial changes in the $J_{SC}$ with repeated testing. However, it was observed that the $V_{OC}$ does undergo small increases with repeated electrolyte filling. This observation is consistent with reports of the same effect,[23] attributed to an increase in the conduction band edge potential of $TiO_2$ arising from a loss of surface bound $Li^+$ ions and an increase in the amount of tBP from repeated pumping. We note also that since a similar increase in $R_R$ is observed for the reference devices, some of this $V_{OC}$ increase be due to a reduced electron recombination rate at the $TiO_2$/dye/electrolyte interface.

An additional effect that is likely to contribute towards the observed trends in $J_{SC}$ and $V_{OC}$, especially at small concentrations of $Ag^+$, is the shift in the conduction band edge ($V_{CB}$) of $TiO_2$

due to the adsorption of $Ag^+$ cations on its surface. Previous work reported that, although large cations such as $Cs^+$ and $Rb^+$ cannot intercalate into the $TiO_2$ lattice like the smaller cations such as $Li^+$ and $Na^+$, they can cause a significant upward shift of the $TiO_2$ $V_{CB}$ as a result of a potential drop across the Helmholtz layer formed at the $TiO_2$/dye/electrolyte interface.[24] This typically results in an increase in $V_{OC}$ and a drop in $J_{SC}$, arising from a reduced driving force for electron injection. A further drop in the photocurrent is expected from the fact that larger cations are typically less solvated and can form the Bjerrum-Fuoss pairing with triiodide, lowering the mobility and ionic activity of triiodide ions in solution.[25, 26] *(see Supplementary Fig. 5)* Since these effects scale with ionic radius, we expect the device response to be highly sensitive to the presence of larger cations in the electrolyte. This suggests that other metal-ion species of interest such as $Hg^+$ and $Pb^+$ can sensitively be detected using the proposed system. Selectivity may be achieved by functionalizing the $TiO_2$ surface to allow for specific adsorption of the target analyte, or by using a selectively permeable membrane.

We also considered the reaction between $Ag^+$ and $I^-$, energetically favorable in comparison to the reaction between $I^-$ and the oxidized dye molecule, which could slow down the dye regeneration process by depleting the electrolyte of iodide ions. This effect however, is found to be insignificant within the range of $Ag^+$ concentrations examined in this study, since the concentration of iodide present in the electrolyte is orders of magnitude larger than the largest concentration of $Ag^+$ tested.

An alternative sensing mechanism that may be realized using the demonstrated platform is one wherein the electrolyte is chosen such that the analyte of interest constitutes one part of the redox couple required for normal DSSC operation. In the absence of the analyte, no redox reaction takes would place, and the PV cell would produce virtually no photocurrent. Introducing the

analyte into the electrolyte would then allow the redox reaction to proceed, spiking the photocurrent in proportion to the concentration of the analyte. While the effect of increasing triiodide in the electrolyte on device performance has been studied extensively,[27-29] this simple concept may be adapted to a wide variety of target species by replacing the iodide/triiodide based electrolyte with an alternate one (e.g. based on a $[FeCN_6]^{3-}/[FeCN_6]^{4-}$ or $[Co(bpy)_3]^{2+/3+}$ redox shuttle). Sufficient power conversion efficiencies (PCEs) have already been demonstrated using these electrolyte systems[30-32] to allow for an external circuit element to be modulated in response to detection events. In addition, improved stability and speed of response may be realized *via* the use of non-corrosive and kinetically fast redox couples. Further, water may be employed as the electrolyte solvent with most such redox couples or the liquid electrolyte may be replaced altogether with a hydrogel,[33, 34] to enable the use of such systems in either one of the 'turn on' or 'turn off' configurations for continuous monitoring of metal-ion content in contaminated water.

We note that the metallic deposition on the photoanode cannot be removed without damaging the dye-coated TiO2 film underneath; as a result, the formulation of the sensor demonstrated in this study implies one-time use. However, since the sensing mechanism demonstrated is essentially independent of device area, the size of each sensor can be reduced to, for example, a tenth of it's present size, allowing for an array of 10-100 sensors to be accommodated on a 1" by 1" substrate.[35, 36] Cheap metal foil or plastic can be used to replace the glass substrates, lowering the material cost, as well as flexible form factor for low cost, roll-to-roll fabrication of disposable sensors. With conventional and emerging fabrication approaches (e.g. micromolding / embossing, 3D printing, CNC milling, etc., many of which are also compatible with continuous processing), costs are expected to be essentially independent of the number of sensors, down to in-

dividual sensor size in the 10 micrometer or smaller scale. Individual sensors in arrays of 100 or more can be activated sequentially, spanning a significantly longer overall period of time.

At the same time, there are target analytes for which the detection mechanism proceeds exclusively through cationic effects (discussed previously), without altering the structure of the $TiO_2$ film. Such target analytes physically adsorb to the surface of the $TiO_2$ film for charge compensation, under bias and can be removed simply by flushing the cavity with fresh electrolyte solution. Such regeneration can also be realized for applications wherein the 'turn on' detection mechanism is employed.

In summary, we demonstrated a novel and versatile detection scheme, in which power generation as well sensing is achieved using a single dye-sensitized solar cell device. We found that this scheme can reliably detect small concentrations of charged species in solution, without making substantial modifications to an efficient and well-understood system. Moreover, such a technique can be applied to the detection of a wide variety of metal ions with high sensitivity and selectivity simply by using different material systems to fabricate the cell. Changes in sensor response arising from extraneous factors can be eliminated using simple circuitry (e.g. a bridge or a variant) that compares the responses of a control device and that of a device exposed to the target analyte. This compensating arrangement is standard (and usually extremely compact) for many types of sensors and modulators, where light intensity, temperature, or other variables may be present.[37] Although further efforts are required to arrive at a fully integrated device that is ready for commercialization, the concept discussed here represents an important step toward realizing autonomous, ultra-compact sensing devices.

## Acknowledgements

## Notes and references

*[a]Department of Materials Science and Engineering, University of Michigan, Ann Arbor, Michigan 48109, USA*

*[*]corresponding: mshtein@umich.edu*

Electronic Supplementary Information (ESI) available: [Methods and additional figures]. See DOI: 10.1039/c000000x/

1.  G. Aragay, J. Pons and A. Merkoci, *Chem. Rev.,* 2011, **111**, 3433.

2.  J. F. Zhang, Y. Zhou, J. Yoon and J. S. Kim, *Chem. Soc. Rev.,* 2011, **40**, 3416.

3.  C. J. Chang, J. Jaworski, E. M. Nolan, M. Sheng and S. J. Lippard, *Proc. Natl. Acad. Sci.* 2003*, **101,** 1129.

4.  Y. Choi, Y. Park, T. Kang and L. P. Lee, *Nat. Nano.* 2009, **4**, 742.

5.  F. Long, A. Zhu, H. Shi, H. Wang and J. Liu, *Sci. Rep.,* 2013*, **3**, 2308.

Nanoscale Accepted Manuscript

6. W. Hong, W. Li, X. Hu, B. Zhao, F. Zhang and D. Zhang, *J. Mater. Chem.,* 2011, **21**, 17193.

7. H. Li, J. Zhai and X. Sun, *Langmuir* 2011, **27**, 4305.

8. B. Kumar et al., *Nano Lett.* 2013, **13,** 1962.

9. Y. Ohno, K. Maehashi, Y. Yamashiro and K. Matsumoto, *Nano Lett.* 2009, **9,** 3318.

10. O. Knopfmacher, *Nat. Commun*. 2014, **5**, 2954.

11. K. Schmoltner, J. Kofler, A. Klug and E. J. W. List-Kratochvil, *Adv. Mater.* 2013, **25**, 6895.

12. R. N. Supino and J. J. Talghader, Autonomous metal ion sensors. in: *MEMS 2006: 19th IEEE International Conference on Micro Electro Mechanical Systems, Technical Digest, IEEE, New York,* 2006*, pp.* **370–373**.

13. B. O'Reagan and M. Grätzel, *Nature* 1991, **353**, 737.

14. M. Grätzel, Photoelectrochemical cells. *Nature* 2001, **414**, 338.

15. A. Hagfeldt, G. Boschloo, L. Sun, L. Kloo and H. Pettersson, *Chem Rev.* 2010, **110,** 6595.

16. J. D. Uram, K. Ke, A. J. Hunt and M. Mayer, *Small* 2006, **2**, 967.

17. E. C. Yusko et al., *Nat. Nano.* 2011, **6**, 253.

18. R. Kern, R. Sastrawan, J. Ferber, R. Stangl and J. Luther, *Electrochimica Acta* 2002, **47**, 4213.

19. Q. Wang, J. E. Moser and M. Grätzel, *J. Phys. Chem. B* 2005*,* **109**, 14945.

20. B. A. Gregg, F. Pichot, S. Ferrere and C. L. Fields, *J. Phys. Chem. B* 2001, **105**, 1422.

21. M. K. Nazeeruddin et al., *J. Am. Chem. Soc.* 1993, **115**, 6382.

22. G. Boschloo and A. Hagfeldt, *Acc. Chem. Res.* 2009, **42,** 1819.

23. K. Miettunen, P. R. F. Barnes, X. Li, C. H. Law and B. C. O'Regan, *J. Electroanal.*

*Chem.* 2012, **41**, 677.

24. B. Enright, G. Redmond and D. Fitzmaurice, *J. Phys. Chem.* 1994, **98**, 6195.

25. Y. Liu, A. Hagfeldt, X. R. Xiao and S. E. Lindquist, *Sol. Energ. Sol. Mat. C.* 1998, **55**, 267.

26. H. Lindström et al., *J. Phys. Chem. B* 1997, **101**, 7710.

27. S. Nakade et al., *J. Phys. Chem. B* 2005, **109**, 3480.

28. J. L. Lan, T. C. Wei, S. P. Feng, C. C. Wan and G. Cao, *J. Phys. Chem. C* 2012, **49**, 116.

29. A. Mathew, V. Anand, G. M. Rao and N. Munichandraiah, *Electrochimica Acta* 2013, **87**, 92.

30. T. Daeneke et al., *Adv. Mater.* 2012, **24**, 1222.

31. J. H. Yum et al., *Nat. Commun.* 2012, **3**, 631.

32. W. Xiang, F. Huang, Y. B. Cheng, U. Bach and L. Spiccia, *Energy Environ. Sci.* 2013, **6**, 121.

33. S. J. Park et al., *ACS Nano* 2013, **7**, 4050.

34. W. Xiang, W. Huang, U. Bach and L. Spiccia, *Chem. Commun.* 2013, **49**, 8997.

35. W. Guo, X. Xue, S. Wang, C. Lin and Z. L. Wang, *Nano Lett.* 2012, **12**, 2520.

36. S. Cho, H. Park, M. Kim, S. Kim and S. Lee, *Nanoscale Res. Lett.* 2013, **8**, 491.
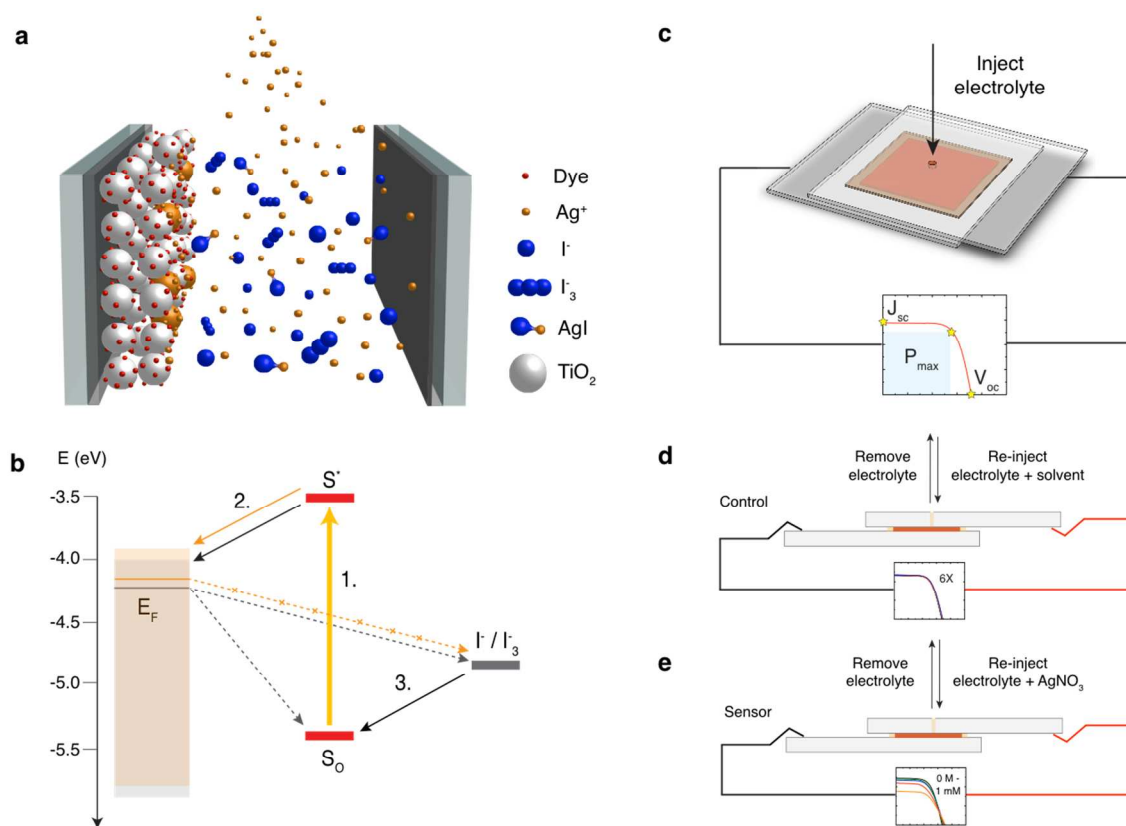
37. Mandalakas J. N., U. S. Patent 3,480,781 (1969).

**Fig. 1. (a)** Schematic of a dye sensitized photovoltaic cell responsive to the presence of ionic species such as silver by producing a change in its electrical characteristics. For example, introducing silver ions into the electrolyte of a normally operating DSSC results in the adsorption of Ag ions as well as the formation of metallic precipitates on the mesoporous $TiO_2$ electrode, shown here in orange. **(b)** An energy level diagram, showing how the processes described in part (a) alter key steps in the device operation. The solid black lines represent the forward processes in normal DSSC operation while the black dotted lines represent the possible recombination pathways in the system. Shown in orange is how the adsorption of Ag ions may shift the conduction band potential of the $TiO_2$ and reduce the driving force for charge injection while the formation of metallic precipitates can render dye sites inactive and block recombination between electrons injected into the $TiO_2$ and triiodide ions in the electrolyte. These effects are discussed

in detail in the results section. **(c)** Schematic of the testing protocol for the control and sensor tests performed in this study. Step 1: The electrolyte is introduced into the cavity using a vacuum syringe and the device characteristics are measured. **(d)** Step 2 (Control): The electrolyte is sucked out of the cavity and the electrolyte + acetonitrile is vacuum filled into the cavity; device characteristics are measured. This step is repeated several times on the same device. **(e)** Step 2 (Sensor): The electrolyte is extracted out of the cavity using the syringe and the electrolyte + $AgNO_3$ dissolved in acetonitrile, is vacuum filled into the cavity; device characteristics are measured. This step is repeated for each concentration of $Ag^+$ on the same device.
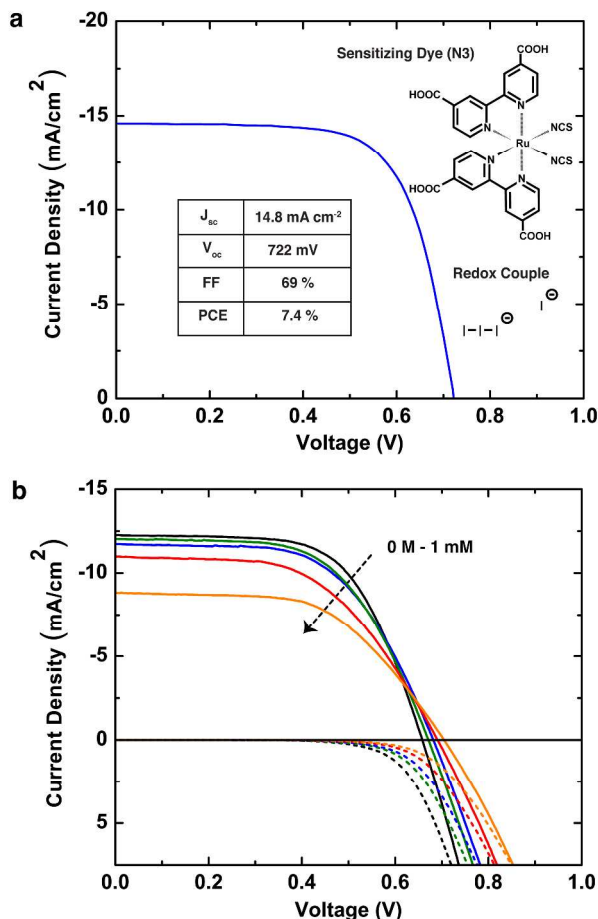
**Fig. 2. (a)** Current density-voltage (J-V) characteristics of a high efficiency DSSC based on (cis-bis(isothiocyanato)bis(2,2′-bipyridyl-4,4′-dicarboxylato)-ruthenium (II) dye (N3) and iodide/triiodide in acetonitrile) fabricated in this study, under AM 1.5 (100 mW/cm$^2$) simulated sunlight. The area of the dye coated TiO$_2$ region was 0.1 cm$^2$. *Inset:* Schematic showing the molecular structures of the sensitizing dye and redox shuttle used along with the obtained performance parameters for one such device. Nominal power conversion efficiency (PCE) = 7.4%, fill factor (FF) = 69%, short circuit photocurrent ($J_{SC}$) = 14.8 mA/cm$^2$, and open circuit voltage ($V_{OC}$) = 0.722 V. **(b)** JV characteristics of a device for which AgNO$_3$ dissolved in acetonitrile is added to the electrolyte at varying concentrations. From top to bottom, the bold lines represent curves under illumination while the dotted lines represent curves in the dark for 0 M, 1 μM, 10 μM, 100 μM and 1 mM [Ag$^+$] respectively.
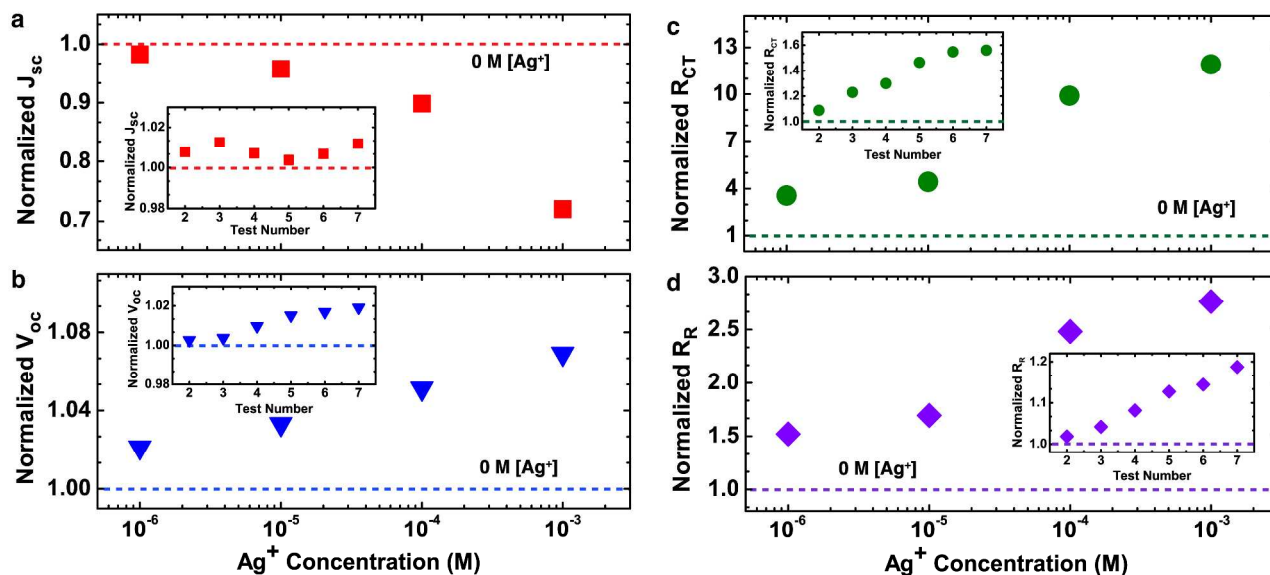
14

**Fig. 3. (a)** Changes in short-circuit current density as a function of $[Ag^+]$. *Inset:* Changes in $J_{SC}$ for a reference device that is repeatedly tested in a manner analogous to the sensor. These variations were found to be negligible. **(b)** Changes in $V_{OC}$ as a function of $[Ag^+]$. *Inset:* $V_{OC}$ for the reference devices shows a steady increase with repeated testing, smaller in magnitude to $V_{OC}$ changes observed from the effect of Ag addition. **(c)** Fitted changes in the charge transfer resistance at the counter electrode ($R_{CT}$), plotted as a function of $[Ag^+]$. *Inset:* $R_{CT}$ for the reference devices. **(d)** Fitted changes in resistance at the $TiO_2$/dye/electrolyte interface ($R_R$) obtained via EIS measurements, plotted as a function of $[Ag^+]$. *Inset:* $R_R$ for the reference devices.
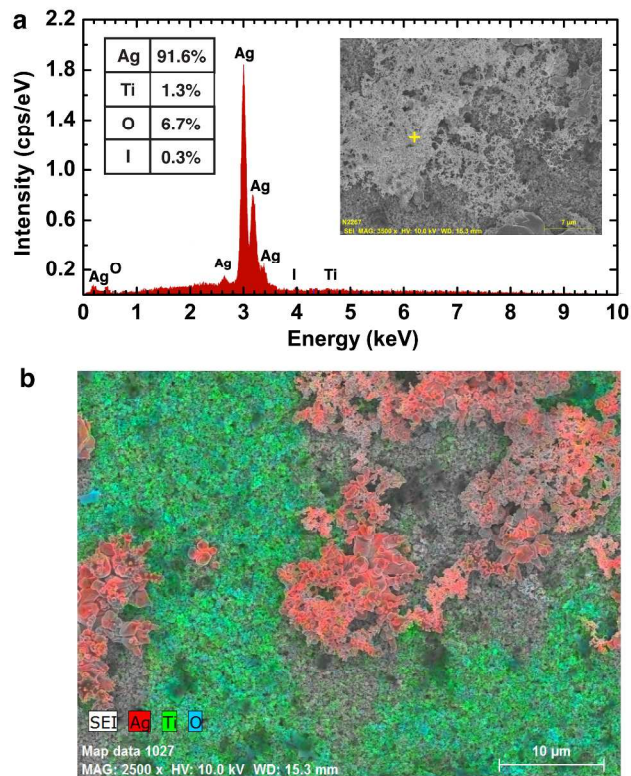
15

**Fig. 4. (a)** EDS spectrum obtained for the region marked with a yellow cross on the SEM image of the $TiO_2$ electrode. *Inset:* Relative atomic weight percentages of the four primary elements expected to be present on the electrode surface. The high percentage of silver is indicative of the fact that silver clusters are indeed formed on the electrode. **(b)** EDS mapping overlaid on an SEM image of the electrode, showing Ag rich regions in red and $TiO_2$ rich regions in blue/green.